TU Delft

Delft University of Technology

Experimental validation of a model for prediction of dynamic ice-structure interaction

Hendrikse, H.; Ziemer, G.; Owen, C. C.

DOI
10.1016/j.coldregions.2018.04.003

Publication date
2018

Document Version
Final published version

Published in
Cold Regions Science and Technology

Citation (APA)
Hendrikse, H., Ziemer, G., & Owen, C. C. (2018). Experimental validation of a model for prediction of dynamic ice-structure interaction. *Cold Regions Science and Technology*, *151*, 345-358. https://doi.org/10.1016/j.coldregions.2018.04.003

Important note
To cite this publication, please use the final published version (if applicable).
Please check the document version above.

Copyright
Other than for strictly personal use, it is not permitted to download, forward or distribute the text or part of it, without the consent of the author(s) and/or copyright holder(s), unless the work is under an open content license such as Creative Commons.

Takedown policy
Please contact us and provide details if you believe this document breaches copyrights.
We will remove access to the work immediately and investigate your claim.

This work is downloaded from Delft University of Technology.
For technical reasons the number of authors shown on this cover page is limited to a maximum of 10.

Green Open Access added to TU Delft Institutional Repository

'You share, we take care!' - Taverne project

https://www.openaccess.nl/en/you-share-we-take-care

Otherwise as indicated in the copyright section: the publisher is the copyright holder of this work and the author uses the Dutch legislation to make this work public.

Cold Regions Science and Technology 151 (2018) 345–358

Contents lists available at ScienceDirect

Cold Regions Science and Technology

journal homepage: www.elsevier.com/locate/coldregions

Experimental validation of a model for prediction of dynamic ice-structure interaction

H. Hendrikse[a,*], G. Ziemer[b], C.C. Owen[a]

[a] Delft University of Technology, The Netherlands
[b] HSVA, Germany

ARTICLE INFO

Keywords:
Ice-induced vibrations
Model-scale experiments
Analytical model
Frequency lock-in

ABSTRACT

Vertically sided offshore structures subjected to level ice are designed to withstand the effects of ice-induced vibrations. Such structures are, for example, offshore wind turbines on monopile foundations, multi-legged oil- and gas platforms or lighthouses. For the prediction of dynamic interaction between ice and structures, several phenomenological models exist. The main challenge with these models is the limited amount of data available for validation, which makes it difficult to determine their applicability. In this study, an attempt is made to validate one of the existing models. First, the parameters which define the ice in the model were derived from new model-scale experiments with a rigid rectangular structure. The model was subsequently applied to simulate the interaction between ice and two compliant rectangular structures with different structural properties. Finally, model-scale experiments were conducted for the two compliant structures. Results of the experiments and model were compared to assess the capability of the model to predict dynamic ice-structure interaction. Results show that the adopted approach allows for a definition of the input parameters of the model and accurate prediction of frequency lock-in and continuous brittle crushing for compliant structures. Intermittent crushing was not observed in the model-scale experiments due to the model-scale ice bending significantly during low ice speeds. As a consequence, the model could not be validated for this regime of interaction. The approach followed and challenges encountered during its application are discussed.

1. Introduction

Dynamic interaction between a floating ice sheet and a vertically sided offshore structure can result in ice-induced vibrations. These structural vibrations require attention in the design of offshore structures for both ultimate and fatigue limits (ISO19906, 2010). In the past, ice-induced vibrations have been observed for offshore oil- and gas platforms and navigational aids such as lighthouses, resulting in failure of structural members and adverse working conditions (Bjork, 1981; Jefferies and Wright, 1988; Yue and Li, 2003). With recent offshore wind developments in the Baltic Sea and Bohai Bay, the interaction between sea ice and offshore wind turbines has intrigued researchers.

For the design of offshore structures at locations where level ice may be present, the ability to accurately predict the interaction between sea ice and structure is required. The main challenge is predicting the occurrence of the three known regimes of ice-induced vibrations: intermittent crushing, frequency lock-in, and continuous brittle crushing (ISO19906, 2010). Each of the regimes has a specific impact on the structure. Intermittent crushing results in the largest global loads on the structure and frequency lock-in generally results in the most significant contribution to fatigue damage, whereas continuous brittle crushing results in the smallest global ice loads but likely contributes to fatigue as this regime is observed most frequently.

Due to the complexity of the interaction, only approximations based on empirical formulas (Huang et al., 2007; ISO19906, 2010; Palmer et al., 2010; Guo, 2013) and phenomenological models exist (Sodhi, 1994; Kärnä et al., 1999; Määttänen, 1999; Hendrikse and Metrikine, 2016; Ji and Oterkus, 2016). One of the challenges with the existing models is to determine their range of applicability. There are only limited full-scale and model-scale data available against which the models can be validated. Each of the theories and models predicts the interaction to develop differently for different types of structures in varying ice conditions. This presents a risk of inaccurate prediction of the response of structures with significantly different structural properties than those limited cases for which the models have been shown to be applicable.

Application of full-scale data for validation of numerical models is challenging. First of all, few full-scale data sets exist which contain

* Corresponding author.
E-mail address: h.hendrikse@tudelft.nl (H. Hendrikse).

https://doi.org/10.1016/j.coldregions.2018.04.003
Received 17 November 2017; Received in revised form 22 February 2018; Accepted 4 April 2018
Available online 06 April 2018
0165-232X/ © 2018 Elsevier B.V. All rights reserved.

measurements of all regimes of interaction. Furthermore, the data sets often suffer from inaccuracies arising from several sources including incomplete load and response monitoring, and inhomogeneous, deficiently measured ice properties. Model-scale experimental campaigns have resulted in important insights and data with respect to ice-induced vibrations (Sodhi and Morris, 1984; Tsuchiya et al., 1985; Timco, 1987; Singh et al., 1990; Sodhi, 2001; Takeuchi et al., 2001; Määttänen et al., 2012; Ziemer and Evers, 2016). However, there are several challenges regarding the application of reported results for validation of models. The main challenge is that, often, not all of the input parameters of the models can be determined based on the reported results. In that case, care must be taken to avoid that validation instead becomes a model fitting exercise. The second challenge is that during model-scale experiments, the structural properties or ice properties are usually not varied significantly; thus, extreme parameter combinations are not available to determine the limitations of models. It is known that, in case intermittent crushing or frequency lock-in develop, the measured ice load contains a significant non-linear dependence on the interaction between ice and structure. Therefore, ice load time histories obtained from such experiments can rarely be used to validate the description of the ice in the models. This final challenge can be overcome by performing experiments with structures which are close to being rigid, thereby preventing the interaction between ice and structure from influencing the experimental results.

In this study, validation of the model by Hendrikse (2017) is attempted based on an approach introduced by Hendrikse and Metrikine (2016). The approach consists of three steps, the first of which is to define the parameters which describe the ice in the model based on results from model-scale experiments with a rigid structure. The model is then applied to simulate the interaction between ice and compliant structures. The final step is to validate the capability of the model to predict the dynamic ice-structure interaction for the compliant structures by model-scale experiments. If successful, it is demonstrated that the model can predict the interaction between the model ice used and compliant structures, and that there is a way to determine the input parameters of the model a-priori from dedicated experiments with a rigid structure. The experiments of this study were conducted in the Large Ice Tank at the Hamburg Ship Model Basin (HSVA) testing facility in December 2016 as part of the 'Ice-Induced Vibrations of Offshore Structures' (IVOS) project (Ziemer, 2017).

The article is structured as follows. In Section 2, the experimental setup, analytical model, and approach for determining the input parameters of the model are introduced. Section 3 describes the results from the experiments with a rigid structure. These results are used in Section 4 to determine the ice related input parameters of the numerical model. In Section 5, the model is then applied for two scenarios where flexible structures interact with the ice. Simulation results are compared to experimental data. The obtained results are discussed in Section 6, which is followed by the conclusion.

2. Description of the model-scale experiments and analytical model

Here the experiments are introduced, providing a description of the setup and the general characteristics of the ice and structures used. The analytical model is briefly described, followed by the approach for determining the input parameters of the model based on experiments with a rigid structure.

2.1. Model-scale indentation experiments with rigid and flexible rectangular indenters

Model-scale indentation experiments were conducted in the Large Ice Tank at the Hamburg Ship Model Basin (HSVA) testing facility in December 2016 as part of the 'Ice-Induced Vibrations of Offshore Structures' (IVOS) project (Ziemer, 2017). An overview of the test parameters is given in Table 1 and the structural setup is shown in Fig. 1.

Table 1
Overview of test parameters.

	Rigid	Flexible 1	Flexible 2
Structure width [m]	0.2	0.2	0.2
Ice thickness [m]	0.052	0.048	0.045
Flexural strength [kPa]	48	58	60
Uniaxial compressive strength [kPa]	100	115	110
Density [kg m^{-3}]	896	896	884
Salinity [‰]	4.0	4.0	3.8
Waterline stiffness [kN m^{-1}]	–	1290	1950
Natural frequency [Hz]	–	4.2	5.4
Damping ratio [−]	–	0.014	0.014

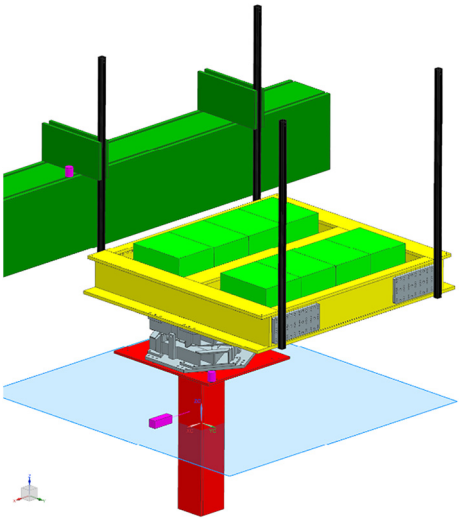

Fig. 1. Illustration of the compliant test setup. The rectangular indenter is shown in red. It is connected to a six-component load scale which is connected to a compliant basis indicated in yellow. Removable masses are indicated in light green and in black four bending rods are indicated which control the stiffness of the setup. The location of the laser and accelerometers is indicated by pink boxes. (For interpretation of the references to colour in this figure legend, the reader is referred to the web version of this article.)

One rigid structure and two compliant structures with different structural properties were tested in two ice sheets. All structures had rectangular cross-sections with a side length of 0.2 m. The rectangular shape was chosen to create a one-dimensional interaction between ice and structure. The compliant setup consisted of a compliant base attached to the main carriage of HSVA's Large Ice Tank by bending rods. The rectangular structures were mounted to this base by a 6-component load scale to measure the global forces and bending moments. Different structural properties could be obtained by varying the added weights and by changing the number and length of the bending rods. For the rigid setup, the structure was attached to the main carriage by a steel girder. The 6-component scale was removed to further reduce the compliance of the setup. Displacement of the model structure was, in both cases, measured with respect to the main carriage with a laser displacement transducer, and accelerations of the structure and carriage were measured by accelerometers. At the ice-structure interface, Tekscan tactile sensors were installed to measure local pressures. Both a detailed sensor (Type 5101, 15.5 sensels cm^{-2}) and a rough sensor (Type 5260, 2.3 sensels cm^{-2}) with a scan rate of 300 Hz were used to capture the global pressures and provide a zoom-in on local pressures.

The experiments were performed in a columnar grained model ice sheet which was produced in NaCl-doped water with a salinity of 7‰ by means of seeding. The air temperature was −18 °C during the growth process. Air bubbles were embedded in the growing ice sheet to

ensure the brittle behavior of the ice as described by Evers and Jochmann (1993). Subsequent to the ice growth process, the temperature was raised to hit the target ice thickness of 0.05 m and target ice properties. Table 1 shows the average properties. The uniaxial compressive strength tests were performed at a strain rate of $10^{-3}\,s^{-1}$. At the locations where the samples were taken, flexural strength tests were also performed. During the tests, the ice remained frozen to the basin walls to provide confinement and the structures were moved through the ice using the main carriage.

At the start of a testing day, plucking tests were performed to determine the structural stiffness, and the natural frequency, and damping ratio of the first mode. The design of the setup was such to give a large separation between the natural frequencies of the first two modes. This was done to permit a single-degree-of-freedom representation of the structure in the model simulations. The tests showed, however, that a higher mode oscillation existed at an unintended frequency about three times the first natural frequency, which appears to have resulted from the attachment of the structure to the load transducer. The ratio of three is still significant, but this second mode may have only slightly influenced the interaction. Additionally, a minor non-linear amplitude dependence of the structural damping was observed. The value of the damping ratio reported in Table 1 is that for an oscillation amplitude of 1 mm. Indentation tests were performed by moving the main carriage and the attached structure at a constant speed. In Table 2, the tested speeds and their increments are reported for each of the tests. Further details of the testing days can be found in Ziemer (2016).

2.2. Model description

The physical basis of the analytical model is treated in detail in Hendrikse (2017). An illustration of the model is shown in Fig. 2. The basic principle of the model is that a large contact between ice and structure develops when ice is loaded slowly, whereas a small contact develops when ice is loaded quickly. To reproduce this physical observation with the model, the ice is portioned into N independent ice elements, each modelled by a combination of springs and dashpots which allows for elastic deformation, inelastic deformation, and local failure of the ice. The model is one-dimensional and local effects such as corner effects for rectangular structures are not explicitly included in the model.

In comparison to our previous work (Hendrikse and Metrikine, 2016), the frictional slider, which was present in the model to allow for plastic deformation of the ice elements, has here become obsolete by introduction of a non-linear dashpot to simulate the creep regime. The introduced non-linearity results in a cubic dependency of the global peak load on ice indentation speed as observed for secondary creep of ice (Ponter et al., 1983). These changes mainly affect the model predictions in the creep regime.

In this study it was decided to model the structure in a simplified manner using a single-degree-of-freedom oscillator. The rectangular structure used in the experiments was designed such that the fundamental and second natural frequency differ significantly; therefore, it can be assumed that most of the interaction between ice and structure occurs in the first mode of the structure. The equation of motion of the structure is given by:

$$\ddot{u}_s + 2\zeta_s\omega_s\dot{u}_s + \omega_s^2 u_s = \frac{F_{ice}(u_s,t)}{M_s} \tag{1}$$

where over-dots represent derivatives with respect to time, and with u_s the displacement of the structure, M_s the structural mass, ζ_s the structural damping as a fraction of critical damping, ω_s the fundamental natural frequency of the structure, and $F_{ice}(u_s,t)$ the global ice load given as the sum of the contributions of individual ice elements i:

$$F_{ice}(u_s t) = \sum_{i=1}^{N} K_2(u_{i,2} - u_{i,1})\mathrm{H}(u_{i,1} - u_s) \tag{2}$$

with H the Heaviside step function indicating contact or no contact between an ice element and the structure, K_2 the front spring stiffness of the ice elements, and N the total number of ice elements. Each ice element has three degrees of freedom $u_{i,1}$, $u_{i,2}$, and $u_{i,3}$, for which the equations of motion are given by:

$$\begin{aligned} u_{i,1} &= \begin{cases} u_{i,2} & u_{i,1} < u_s \\ u_s & u_{i,1} \geq u_s \end{cases} \\ \dot{u}_{i,2} &= \frac{K_2}{C_1}(u_{i,1} - u_{i,2}) + \frac{K_1}{C_1}(u_{i,3} - u_{i,2}) + v_{ice} - \frac{1}{C_2}(K_2(u_{i,2} - u_{i,1}))^3 \\ \dot{u}_{i,3} &= v_{ice} - \frac{1}{C_2}(K_2(u_{i,2} - u_{i,1}))^3 \end{aligned} \tag{3}$$

with v_{ice} the ice drift velocity towards the structure, K_1 and C_1 the linear spring and dashpot coefficients of the middle part of the ice element, and C_2 the coefficient of the non-linear rear dashpot [$\mathrm{N^3\,m^{-1}\,s}$].

Initial positions for the elements with respect to the structure are drawn from a uniform distribution U:

$$u_{i,1} = u_{i,2} = u_{i,3} = u_{s,0} - \mathrm{U}(0, r_{max} + v_{ice}t_f(v_{ice})) \tag{4}$$

with r_{max} the maximum offset of an element with respect to the structure, $u_{s,0}$ the initial position of the structure, and $t_f(v_{ice})$ the time between initial contact and failure for an individual ice element at the given ice velocity assuming a non-moving structure obtained by solving Eq. (3). The contribution $v_{ice}t_f(v_{ice})$ is added to ensure that the initial distribution of elements is similar to the distribution occurring during interaction. The elements fail as soon as the deformation in the front spring reaches a predefined deterministic critical deformation δ_f:

$$u_{i,2} - u_{i,1} = \delta_f \tag{5}$$

Upon failure of an element i, the element is repositioned relative to the structure with a uniformly distributed offset value:

$$u_{i,1} = u_{i,2} = u_{i,3} = u_s(t) - \mathrm{U}(0, r_{max}) \tag{6}$$

with r_{max} the maximum offset. The equations of motion are solved in the time domain using a 4th order Runge-Kutta scheme with event detection to handle contact and failure. An adaptive time-stepping scheme is used to optimize the time step which can become very small at high velocities as all individual crushing events need to be processed.

2.3. Method of defining the ice input parameters of the model

The model requires definition of eight parameters describing the ice behavior. These parameters are N, K_1, K_2, C_1, C_2, δ_f, r_{max}, and v_{ice}. Of these parameters, v_{ice} can be straightforwardly defined and the remaining seven parameters can be derived from experimental or full-scale measurements of ice action against a rigid structure. The measurements used to define the model input are further referred to as "reference measurements" indicated by subscript *ref*. Once obtained, the parameters describing the ice in the model can be applied for simulations with different structures and ice conditions. It should ultimately be possible to define the model parameters based on physical property measurements of the ice in question. However, research into defining the relationships between physical ice properties and global

Table 2
Indentation speed tested for each structure.

	Rigid	Flexible 1	Flexible 2
Indentation speed (increment) [$\mathrm{mm\,s^{-1}}$]	3–10 (1) 15–50 (5) 60–150 (10) 200 (−)	25 40–45 (1) 50–100 (5) 110–150 (10)	3–50 (1) 60–80 (10) 100 (−) 150 (−)

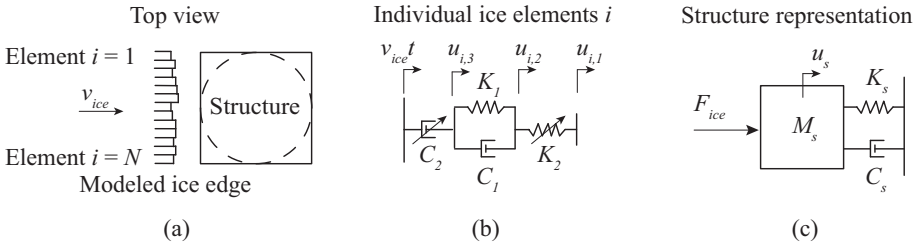

Fig. 2. Illustration of the analytical model. Top view indicating the individual ice elements and structure which can be of various shapes (a), Individual ice elements showing the degrees of freedom with diagonal arrows indicating non-linear elements (b), and the structure modelled here as a single-degree-of-freedom oscillator (c).

ice deformation and failure behavior has not matured enough to yield results.

The reference measurements which can be used to define the ice-related input parameters of the model were previously defined in Hendrikse and Metrikine (2016). The approach is repeated here for completeness. A rigid structure is considered with given width (or diameter) d_{ref}, and shape s_{ref}, in ice defined by its mean thickness h_{ref} and compressive strength σ_{ref}. In he presented study, σ_{ref} was obtained from ex-situ uniaxial compressive strength tests of beam-shaped specimens at $10^{-3}\,s^{-1}$ strain rate. For these reference conditions, the numerical model gives the dependence of global ice load on indentation velocity as illustrated in Fig. 3.

Six out of seven model parameters are found based on six measured quantities indicated by the dots in Fig. 3. The first is the transition speed for which the transition between creep and crushing occurs $v_{t,ref}$. The second is the maximum global load $F_{max,ref}$ which can develop for an indentation velocity equal to the transition velocity. The third and fourth are the mean global load $F_{mean,ref}(v_{ice} \to \infty)$ and standard deviation of the global load $F_{std,ref}(v_{ice} \to \infty)$ in crushing for high velocities. High velocities are, in this case, velocities significantly above the transition from creep to crushing. In crushing, the mean and standard deviation of the global load have been shown to approach a constant value at high indentation speeds in previous experiments (Sodhi and Morris, 1984). The fifth and sixth measured quantities, $F_{mean,ref}(v_1)$ and $F_{mean,ref}(v_2)$, define the gradient of the mean global load dependence on velocity. Alternatively, one measurement in the creep range can be used as shown in Hendrikse and Metrikine (2016).

The seventh and last required measurement concerns the local failure behavior in crushing. An average value for the critical deformation of a single contact zone of the ice $\delta_{f,avg,ref}$ is used. Previous attempts to define this parameter based on the spectrum of the global ice load during high velocity crushing were unsuccessful. The challenge is that, in practice, load signals are often of short duration and show

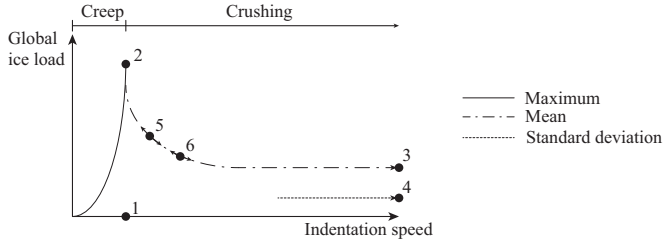

Fig. 3. Dependence of global ice load on indentation speed in the model for a rigid reference structure in reference ice conditions. Trends of the statistical measures are only shown in relevant ranges. Numbered dots indicate the reference measurements required to define the ice in the model, 1: the transition speed, 2: the maximum global load at the transition speed, 3: the mean global load in crushing at high indentation speed, 4: the standard deviation of global load in crushing at high indentation speed, 5 and 6: the mean global load in the transition range for an indentation speed v_1 and v_2. The seventh measurement required is one of the local deformation of the ice before failure which is not depicted in the illustration.

global low frequency variations due to natural variations in ice properties. This results in spectra which do not show a clear frequency band in which local failure occurs. Furthermore, the phenomenological model assumes a constant value of local deformation, strength, and a uniform distribution of the offset. In reality, all three parameters are likely to follow a distribution and perhaps show some degree of correlation. Sensitivity to the choice of critical deformation is further treated in the discussion section.

Based on the seven measured quantities, the seven model input parameters for the reference case can be obtained by solving the following set of equations:

$$
\begin{aligned}
&v_{t,ref} = \frac{1}{C_{2,ref}}(K_{2,ref}\,\delta_{f,ref})^3\\
&F_{max,ref} = N_{ref}\,K_{2,ref}\,\delta_{f,ref}\\
&F_{mean,ref}\,(v_{ice} \to \infty) = N_{ref}\,K_{2,ref}\,\frac{\int_0^{t_f(v_{ice})} u_{i,2}\,(t)\mathrm{d}t}{\frac{0.5r_{max,ref}}{v_{ice}} + t_f\,(v_{ice})}\\
&F_{std,ref}\,(v_{ice} \to \infty)\\
&= \sqrt{N_{ref}\left(\frac{K_{2,ref}^2\int_0^{t_f(v_{ice})}(u_{i,2}\,(t))^2\mathrm{d}t}{\frac{0.5r_{max,ref}}{v_{ice}} + t_f\,(v_{ice})} - \frac{(F_{mean,ref}\,(v_{ice} \to \infty))^2}{N_{ref}}\right)}\\
&F_{mean,ref}\,(v_1) = N_{ref}\,K_{2,ref}\,\frac{\int_0^{t_f(v_1)} u_{i,2}\,(t)\mathrm{d}t}{\frac{0.5r_{max,ref}}{v_1} + t_f\,(v_1)}\\
&F_{mean,ref}\,(v_2) = N_{ref}\,K_{2,ref}\,\frac{\int_0^{t_f(v_2)} u_{i,2}\,(\mathrm{t})\mathrm{d}t}{\frac{0.5r_{max,ref}}{v_2} + t_f\,(v_2)}\\
&\delta_{f,avg,ref} = \delta_{f,ref}
\end{aligned}
\tag{7}
$$

Eq. (7) is defined based on the statistical properties of the model and its derivation is treated in detail in Hendrikse (2017). For different structures in different ice conditions the model parameters are then scaled according to:

$$
\begin{aligned}
&N = N_{ref}\frac{d}{d_{ref}}\\
&K_2 = f_s\,(s, s_{ref})\frac{\sigma}{\sigma_{ref}}\frac{h}{h_{ref}}K_{2,ref}\\
&C_2 = f_s\,(s, s_{ref})\frac{\sigma}{\sigma_{ref}}\frac{h}{h_{ref}}C_{2,ref}\\
&K_1 = f_s\,(s, s_{ref})\frac{\sigma}{\sigma_{ref}}\frac{h}{h_{ref}}K_{1,ref}\\
&C_1 = f_s\,(s, s_{ref})\frac{\sigma}{\sigma_{ref}}\frac{h}{h_{ref}}C_{1,ref}\\
&r_{max} = r_{max,ref}\\
&\delta_f = \delta_{f,ref}
\end{aligned}
\tag{8}
$$

In this way of scaling, the model parameters assume a linear dependence of the mean global load in crushing on h, d, and σ, and a scale factor $f_s(s, s_{ref})$ to reduce or increase the load based on the shape of the structure investigated as compared to the reference shape. Other ratios

are assumed to scale with the mean global load in crushing while maintaining the relative shape of the curves shown in Fig. 3. It remains to be validated to which extent this approach is applicable for values of d and h deviating significantly from h_{ref} and d_{ref}. For ice with significantly different physical properties compared to the reference ice, it has to be considered that the global failure and deformation behavior of the ice under loading depend on the change in physical properties.

3. Results from rigid structure indentation tests

The results from experiments with a rigid rectangular indenter are presented. A qualitative analysis of the observed ice failure process is first given. Challenges with respect to observed flexural failure and its impact on the applicability of the results are described. The rigidity of the test structure is analyzed based on measurements of displacement and acceleration during the tests. Finally, the results obtained with the tactile-sensor measurement system are presented. These results are further used in Section 4 to define the input parameters of the model.

3.1. Qualitative analysis of the observed ice failure process

The aim of the indentation experiments with rigid structures was to investigate the ice failure and deformation behavior in creep and crushing while excluding the effects of interaction between ice and structure. This imposes two requirements on the test setup: low velocity indentation should be possible to reach the creep range, and a relatively stiff ice sheet is required to limit flexural ice motion and bending failure of the ice.

The lowest possible constant speed of indentation that can be achieved with the main carriage in the HSVA ice basin is 3 mm s^{-1}. This velocity was expected to be close to the transitional velocity from creep to crushing, but perhaps not low enough to accomplish a true creep test. The obtained results confirm that crushing occurs at a 3 mm s^{-1} indentation speed (see Fig. 4).

Significant flexural ice motion and flexural failure were observed during the tests. Fig. 4 illustrates the effect of flexural failure on the obtained time trace of the global load. Flexural failure occurred mainly, but not exclusively, in the low velocity experiments. The development of this flexural failure limits the usability of the data as steady-state crushing or full creep interaction cannot develop under conditions where the limiting failure mechanism is bending. A critical assessment of the data is needed to differentiate between trends in global load related to pure crushing and trends related to a combination of crushing and bending of the ice.

In the analysis presented in the remainder of this section, the only time instances considered are those during which steady ice crushing with limited influence of the flexural ice motion was observed. Those time instances were identified by carefully inspecting the time dependencies of the global pressure obtained with the tactile sensor system, as well as the video recordings. Fig. 5 shows an example comparison of a signal before and after the removal of flexural failure associated effects. Table 3 shows the length of the data signals which remained after processing.

3.2. Rigidity of the test structure

It is impossible to design a completely rigid test setup in practice. It is, therefore, important to specify the actual rigidity of the setup to quantify the influence of relative motion between ice and structure on the experimental observations. Dynamic ice-structure interaction is mainly governed by the relative velocity between ice and structure (Määttänen, 1999; Hendrikse and Metrikine, 2016). The rigidity of a structure can therefore be expressed in terms of the occurring relative velocities during indentation. For rigid structures, the minimum relative velocity is approximately equal to the indentation velocity, or ice drift velocity. For flexible structures, the minimum relative velocity can be significantly smaller than the indentation velocity when the structure moves in the direction of the ice.

The structural velocity which occurred during the experiments was derived using both the displacement and acceleration measurements. The acceleration data was filtered by a 2 Hz high-pass filter to remove low frequency contributions leading to drift in the obtained velocity signals. Both acceleration and displacement were re-sampled to 100 Hz. The constant indentation velocity was directly measured as the velocity of the main carriage in the basin.

Fig. 6 shows the obtained minimum relative velocity values for each indentation velocity and the constant indentation velocity. For the minimum relative velocity, the average of ten peak values was chosen to reduce the influence of incidental high velocities on the results. The results from both the displacement and acceleration measurements are fairly consistent. Based on the proximity of all measurement points to the solid line in Fig. 6, the effect of interaction is concluded to be negligible and the structure is confirmed to be rigid.

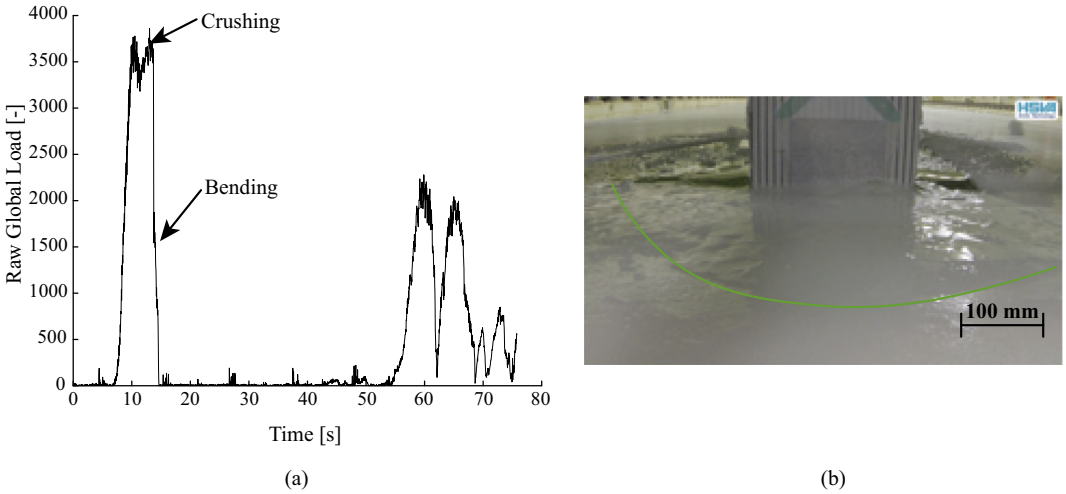

Fig. 4. Plot of the measured global ice load during indentation at 3 mm s^{-1} with the rigid structure (a). The occurrence of local crushing and global bending failure are indicated. A picture to illustrate global bending failure during indentation (b). The green line indicates the water on the ice resulting from the downward flexural motion. (For interpretation of the references to colour in this figure legend, the reader is referred to the web version of this article.)

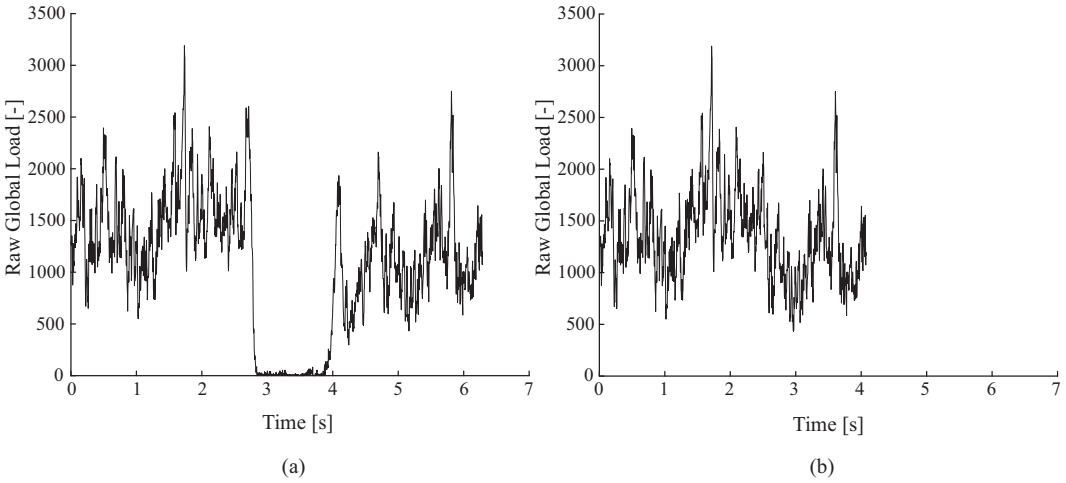

Fig. 5. Effect of removal of time instances associated with flexural ice behavior from the obtained signals. The original measurement (a), the time instances associated with steady crushing at 0.11 m s^{-1} (b).

Table 3
Signal length after removal of flexural failure associated intervals for each of the considered indentation velocities.

Velocity [mm s^{-1}]	3	4	5	6	7	8	9	10	15
Signal length [s]	3.9	27.5	19	2.7	1.3	2.0	4.7	4.3	3.9

Velocity [mm s^{-1}]	20	50	60	70	90	100	110	120	130	140
Signal length [s]	2.7	3.2	3.4	3.9	3.15	4.0	3.9	3.2	2.7	1.3

3.3. Results from the tactile-sensor system

The tactile-sensor system provides information about the local and global ice pressures and ice loads. Of main interest for the determination of the input parameters of the model are the dependence of maximum, mean, and standard deviation of the global ice load on indentation velocity. Global loads can be obtained by summation of the measured pressure in each sensel multiplied by the area of a sensel.

Due to challenges with pre-calibration of the sensor, the obtained pressure values can only be considered in a relative manner in terms of their raw values. However, this does not limit the usability of the data for the purpose of this study. The results in this section are further presented as raw global load values for which the observed ratios are one-to-one related to the ratios for the true global load on the structure. The raw global load is computed by summation of the raw local pressures at a specific time.

In the analysis, only the pressures on the front of the structure directly facing the ice are considered. A low-pass Bessel filter with phase shift correction was applied to the data to remove sensor noise. Fig. 7 shows the obtained values for the mean, maximum, and standard deviation of the raw global load as well as the contact area. The contact area is given by the sum of the number of elements in contact at a specific moment in time.

A typical trend of reducing maximum and mean global load in the low speed range, up to 0.02 m s^{-1}, can be observed. For higher speeds, between 0.05 and 0.14 m s^{-1}, the mean of the global load shows a slight increasing trend with indentation speed. This contradicts earlier findings reported by Sodhi and Morris (1984) who show that the mean global load levels off with increasing indentation speed. An explanation for this difference is found in the increasing trend in the dependence of the statistical measures of the contact area on indentation speed in Fig. 7. This indicates that for higher speeds a larger portion of the tactile

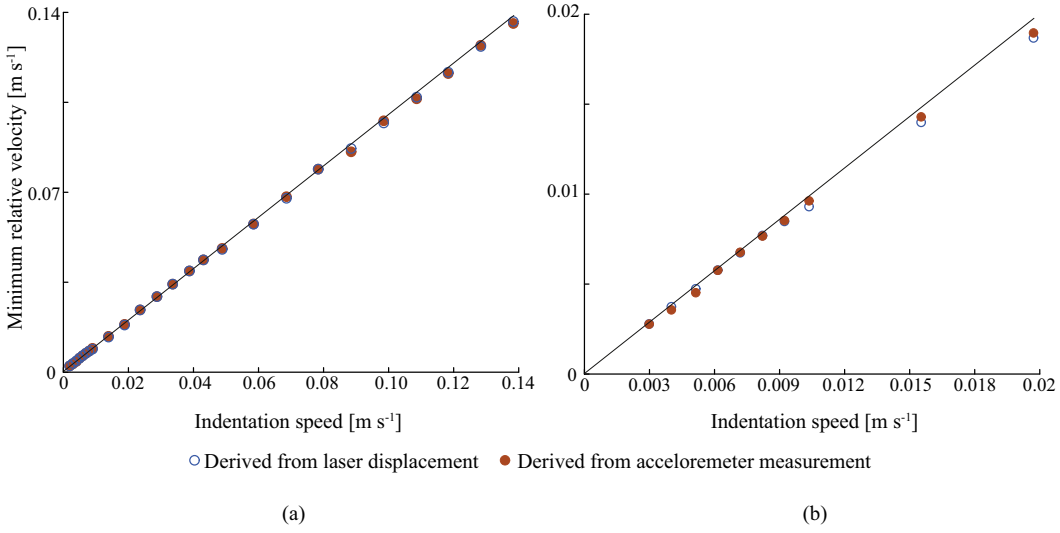

Fig. 6. Minimum relative velocity measured during the experiments (a), and a close-up of the low indentation velocity region (b). The solid line represents the minimum relative velocity for a rigid setup.

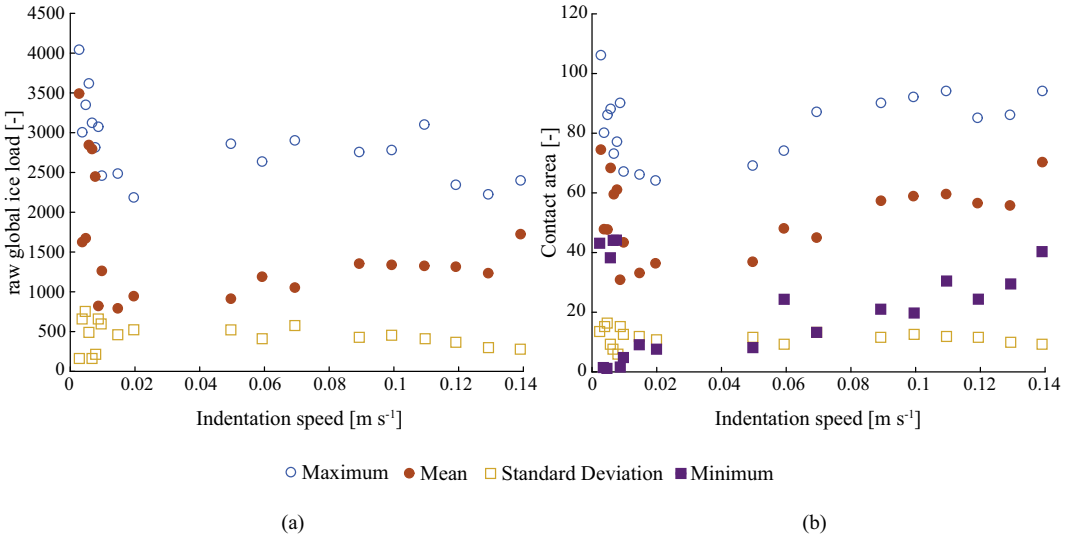

Fig. 7. Dependence of measured raw global load on indentation speed (a), and dependence of measured contact area on indentation speed (b).

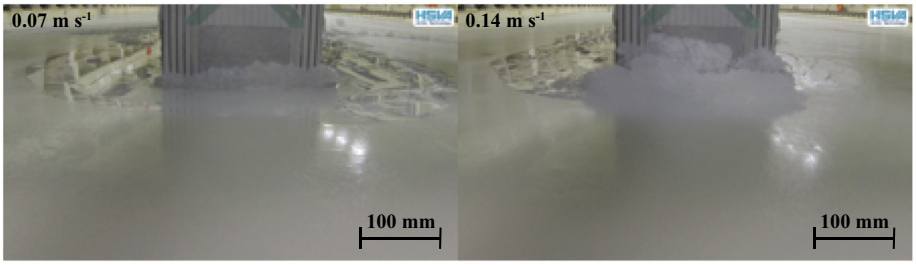

Fig. 8. Pictures of ice rubble resting against the tactile sensor at an indentation speed of 0.07 and 0.14 m s^{-1}.

sensor registers pressure. The reason for this is an increase in ice rubble resting against the sensor, see Fig. 8, resulting in a static contribution to the global load which increases with indentation speed. For the low speed tests, the amount of rubble was significantly less and hence the influence on the results was much smaller.

The ice rubble generates a significantly smaller pressure value in a sensel compared to the intact ice, which should make it relatively easy to distinguish between the two. However, as the ice sheet was oscillating in vertical direction during indentation, the location of the rubble in vertical direction kept changing. A very rough approach to removing the contribution of rubble from the data is to set a minimum pressure threshold. By this approach, not only is the pressure from rubble removed, but also a portion of the pressure from the intact ice. The results after application of this approach with a raw pressure threshold value of 15 are shown in Fig. 9. The raw pressure range for this sensor was between 0 and 255. Comparing the trends in contact area with those shown in Fig. 7, it can be clearly seen that the increasing trend with indentation speed is almost completely gone. The results of the raw global load in Fig. 9 are consistent with the observations reported in literature (Sodhi and Morris, 1984). The effect on the standard deviation of the load is negligible, indicating that indeed a static contribution was removed from the signal.

From the experiment at 0.14 m s^{-1}, the mean raw global load is found to be significantly larger than for the experiments at 0.09 up to 0.12 m s^{-1} while all experiments were in the crushing range. This is a result of the flexural ice motion in the experiments which cannot be completely filtered from the results. The effect is insignificant for high indentation speeds, while for low speeds there is a clear, long period oscillation superimposed on the crushing load. Fig. 10 illustrates that, while the maximum load is in the same range, the minimum loads drop to significantly lower values for the lower ice velocities. The ratios obtained for the experiment at 0.14 m s^{-1} can be considered to reflect pure ice crushing best.

4. Determination of input parameters for the model

The results from indentation experiments with rigid structures are used as reference measurements to determine the input parameters of the model based on the methodology presented in Section 2.3. As only raw global load values were obtained from the pressure sensor, the mean global load in crushing at high velocities cannot be determined from the measurements. It was chosen to scale the raw global load results by dividing with the raw mean global load at 0.14 m s^{-1}. This allows to define six out of seven parameters of the model. In Fig. 11, the scaled raw global loads obtained from the experiment and shown in Fig. 9, are replotted, indicating the reference measurements used for defining the model parameters.

Three reference measurements can be directly obtained from Fig. 11:

$$\begin{aligned}\frac{F_{std,ref}\,(v_{ice}\rightarrow\infty)}{F_{mean,ref}\,(v_{ice}\rightarrow\infty)} &= 0.18\\ \frac{F_{mean,ref}\,(v_1=0.003)}{F_{mean,ref}\,(v_{ice}\rightarrow\infty)} &= 2.29\\ \frac{F_{mean,ref}\,(v_2=0.007)}{F_{mean,ref}\,(v_{ice}\rightarrow\infty)} &= 1.81\end{aligned} \tag{9}$$

The transition velocity and maximum global load at the transition between creep and crushing were not measured in the experiment. A different set of experiments from the IVOS campaign in similar ice conditions (Hinse et al., 2017) showed a transition from creep to crushing in the range between 0.5 and 2 mm s^{-1}. A value of 1 mm s^{-1} is

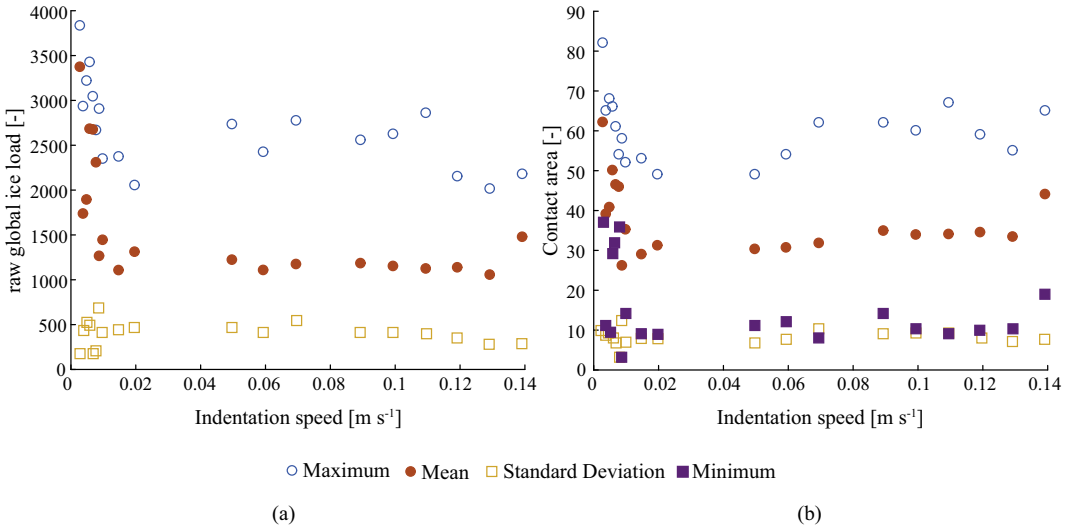

Fig. 9. Raw global load after removal of the ice rubble contribution (a), and contact area measured as the sum of the number of loaded elements after removal of the ice rubble contribution (b).

chosen here as a first estimate. The maximum global load is estimated by extrapolation of the experimental results (see Fig. 11):

$$v_{t,ref} \approx 0.001 \text{ m s}^{-1}$$
$$\frac{F_{max,ref}}{F_{mean,ref}(v_{ice} \rightarrow \infty)} = 3.45 \tag{10}$$

Sensitivity of the model predictions to these two estimations is treated in the Discussion section.

The sixth parameter is the average critical local deformation of the ice $\delta_{f,ref}$. The tactile-sensor system allows for studying individual contact zones to obtain a representative value for this parameter. Fig. 12 shows the distribution of the critical deformation obtained for the test at 0.14 m s^{-1} indentation speed. It was found that the individual contact zones are smaller than the grid resolution of the utilized tactile sensor. Hence, it is impossible to derive a correct distribution of critical deformation of individual contact zones from the measurements. Nevertheless, it is found that the majority of loading events concerned less than 5 mm deformation of the ice and that there is a minimum deformation of about 1 mm. Based on the observations, an estimate of $\delta_{f,ref}$ of 2 mm is made. The sensitivity of the model predictions to this choice is further treated in the discussion section.

Using the reference measurements as input to the system of equations in Eq. (7), the model input parameters are obtained as shown in Table 4. To obtain the parameters, the value of the mean global load measured by the six-component scale during a test at 0.14 m s^{-1} indentation speed with the same structure, but compliant test setup 1 has been used. This mean global load is scaled to account for the difference in uniaxial compressive strength and thickness between the rigid and compliant structure tests. This results in an estimate for $F_{mean,\ ref}(v_{ice} \rightarrow \infty) \approx 1150$ N.

Using the parameters from Table 4, the model is applied to the case of the rigid structure. Results for the global load dependence on velocity are shown in Fig. 13. A good match with the measurement data is obtained, as should be the case. When comparing the model predictions with the experimentally obtained values, the presence of flexural deformation of the model ice sheet is to be considered.

5. Comparison of model predictions and experiments for compliant structures

A comparison of simulation results and model-scale experiments is presented for two cases where model ice interacts with a compliant structure, resulting in the development of ice-induced vibrations. The aim of this comparison is to demonstrate that the model can predict the interaction between ice and structures with different structural properties, using the ice parameters obtained from tests with a rigid

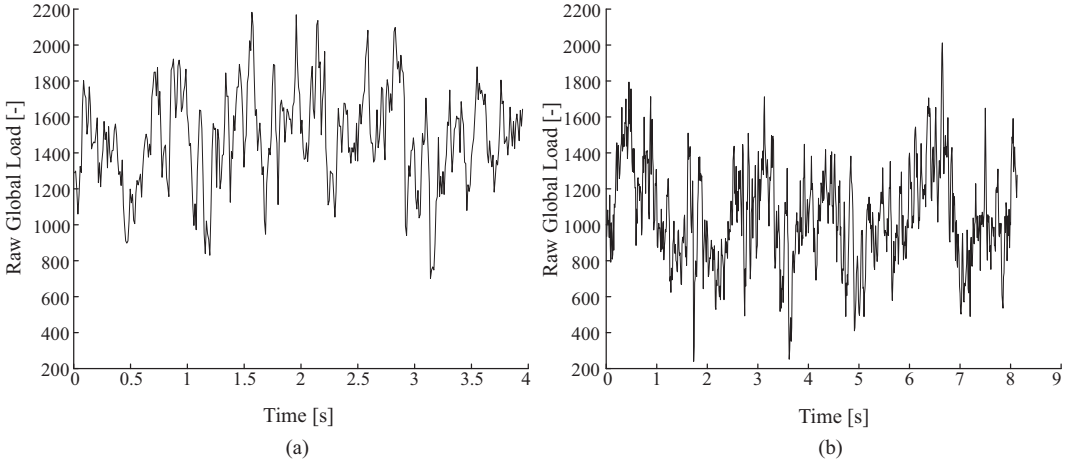

Fig. 10. Time history of raw global load at an indentation speed of 0.14 m s^{-1} (a), and an indentation speed of 0.13 m s^{-1} (b).

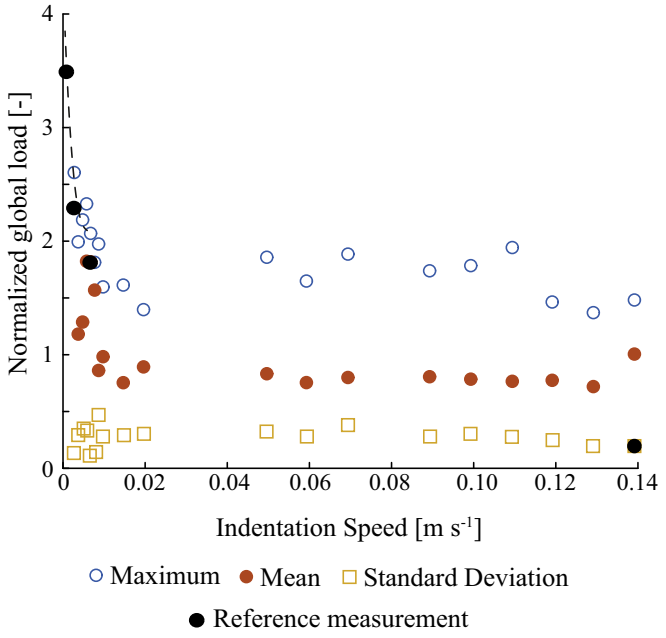

Fig. 11. Replotted results from rigid structure experiments where the loads are normalized with the mean global load from the experiment at 0.14 m s^{-1}. Points from where the reference measurements are obtained are indicated.

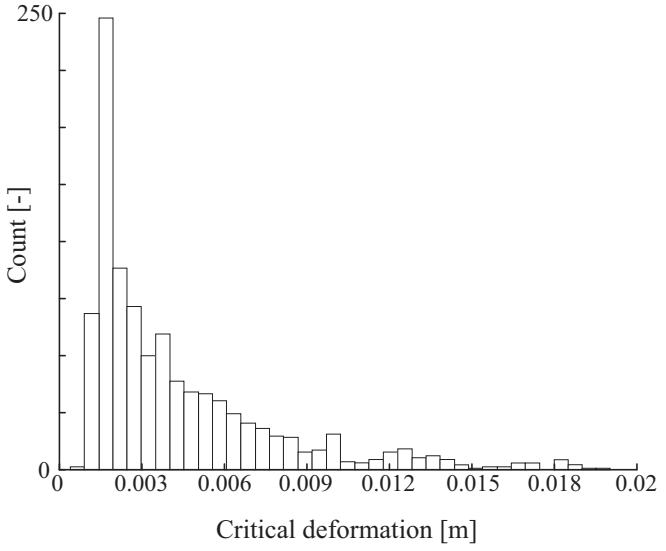

Fig. 12. Distribution of deformation between first contact and failure based on loading of individual sensels of the tactile sensor at an indentation speed of 0.14 m s^{-1}.

Table 4
Derived reference input parameters of the numerical model.

$K_{2,ref}$ [N m^{-1}]	$C_{2,ref}$ [N^3 m^{-1} s]	$K_{1,ref}$ [N m^{-1}]	$C_{1,ref}$ [Ns m^{-1}]	N_{ref} [−]	$r_{max,ref}$ [mm]	$\delta_{f,\ ref}$ [mm]
50,910	1.05 10^9	5372	17,021	39	2.9	2

structure.

The input for the simulations is given in Table 5. The reference parameters, given in Table 4, are used to define the ice in the model. A speed sweep is used for the simulations by increasing the indentation speed stepwise as was done in the model-scale experiments, during which each speed was maintained for about 20 s on average. This is of importance as initial conditions influence the development of frequency lock-in. Simulations were run for at least 20 s, with longer simulation time at low velocities to make sure that a steady-state interaction process developed. In determining statistical measures of the process, only the second half of the obtained signals was used.

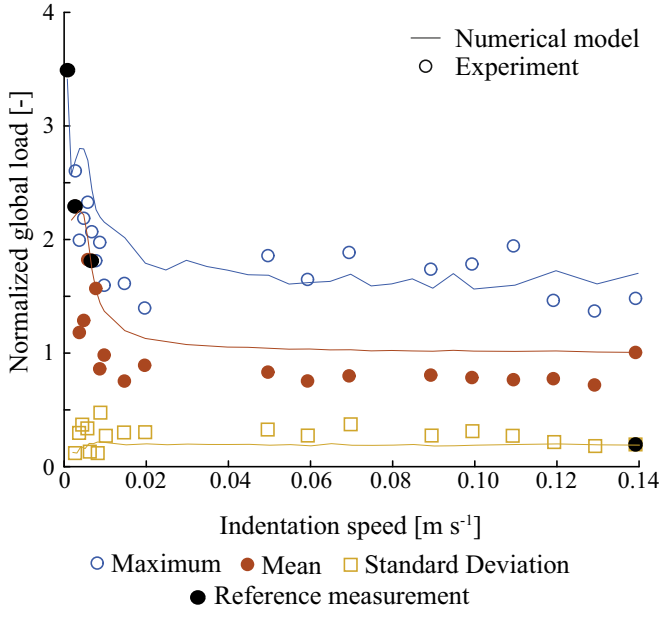

Fig. 13. Comparison between model prediction and experiments for a rigid rectangular structure of 0.2 m width in ice conditions defined in Table 2.

Most of the results from the experiments with compliant structures could be straightforwardly applied as flexural failure impacted only a limited number of tests. The data was processed in a similar manner as for the rigid structure. At low velocities, the interaction was influenced significantly by the occurrence of flexural ice motion which has to be considered in the comparison as the model does not incorporate this behavior. The global ice loads were obtained from the 6-component scale.

The comparison between model predictions and experimental results is presented as follows. On a global level, the statistical measures (mean, maximum, standard deviation) of the global ice load, structural displacement, and structural velocity are compared for different indentation velocities. On a local level, a detailed comparison for a single velocity in the regime of frequency lock-in and the regime of continuous brittle crushing are presented. Comparison in the regime of intermittent crushing is impeded by accompanying flexural motion of the model ice sheet which limits the maximum ice loads.

Fig. 14 shows the ratio between the maximum structural velocity in the direction of ice motion and the indentation speed for the two compliant structures. This plot provides a simple indication of the frequency lock-in range as during frequency lock-in the aforementioned ratio ranges between 1 and 1.5 (Toyama et al., 1983). Fig. 15 shows the trends in global load dependence on indentation speed. Fig. 16 shows the trends in structural displacement. The results are further discussed in the next section.

Fig. 17 shows a comparison of measured and predicted structural displacement and global ice load for a case of frequency lock-in. The signal chosen is the one that matches best in terms of velocity, load, and displacement based on Figs. 14, 15, and 16. Fig. 18 shows a comparison of measured and predicted structural displacement and global ice load in a case of continuous brittle crushing. Results are further discussed in the next section.

Table 5
Input for simulation of the experiments with two compliant structures.

	K_s [kN m^{-1}]	f_s [Hz]	ζ_s [−]	h [m]	d [m]	Shape	σ [kPa]	$f(s,s_{ref})$
Compliant 1	1290	4.2	0.014	0.048	0.2	Rectangular	115	1
Compliant 2	1950	5.4	0.014	0.045	0.2	Rectangular	110	1

6. Discussion

The experimental setup allowed for an easy variation of structural properties by which the required data from rigid and flexible structures could both be obtained. The rigid setup can be considered as rigid, given the ice load level observed in the experiments. Two compliant structures with different structural properties were successfully implemented. The measurement systems installed recorded necessary information about ice loads and structural motion. Despite the impossibility to define the absolute magnitude of the pressures obtained by the tactile sensor, the use of the ratios between raw pressure values still permitted a definition of the model input parameters.

The main challenges, with respect to the experimental data, originated from the use of model ice, which is not designed for tests with pure crushing. The ice tended to bend downwards during interaction, often resulting in flexural failure at low velocities. The influence of this on the results is two-fold. First, the amount of steady-state crushing data gathered during the experiments is reduced as bending failure causes long durations of no loading in the signals (Fig. 4). Second, the load levels measured may be significantly smaller than those associated with pure crushing as previously illustrated analytically for ice buckling (Hendrikse and Metrikine, 2016). The latter effect occurs mainly at low indentation speeds and can prevent the development of intermittent crushing and frequency lock-in. For the rigid structure experiments, it leads to some uncertainty with respect to the mean and maximum global load levels during crushing. Also, the comparison between model predictions and experimental data for compliant structures at low indentation speeds is not possible because of this. The use of a different type of ice, thicker ice, or a smaller size structure can resolve these issues for future tests.

Despite the challenges associated with the measurement system and use of model ice, the obtained experimental results show trends consistent with those reported in literature. For the rigid structure, the maximum and mean global ice loads show a strong decreasing trend with increasing indentation speed for low speeds up to 0.02 m s^{-1}, after which they level off. This is consistent with the results reported by Sodhi and Morris (1984). The compliant structures show frequency lock-in to occur over a range of velocities in which the structural velocity in the direction of ice drift follows a linear relation with the indentation speed as observed previously by Toyama et al. (1983) and Tsuchiya et al. (1985). For the structure with a higher natural frequency and stiffness, compliant structure 2, the indentation speed up to which frequency lock-in developed is smaller than for the structure with a lower natural frequency and stiffness. This is consistent with the results reported by Huang et al. (2007).

The obtained data from the rigid structure experiments could be straightforwardly applied to define the model input parameters. The missing data for the transition velocity, maximum global load, and mean global load in crushing could be estimated with a small uncertainty. The main difficulty is to determine the critical deformation of the ice in the model. An estimation has been made based on the indentation velocity and the time during which individual sensels of the tactile sensor registered contact. As the contact measurements included ice rubble and multiple-zones could have been in contact with a single sensel this approach did not allow for an accurate estimation. Future studies with more detailed tactile sensors may reveal the true distributions of critical deformation, offset, and local maximum pressure. Once those are available, the model can be adjusted to account for these more realistic distributions. It is noted, however, that the model is phenomenological and already shows to capture the interaction on a global scale. A very detailed description of the local failure process may not necessarily change the model predictions significantly.

The comparison between model predictions and experimental results for flexible structures, shown in Section 5, illustrates that the model can describe the dynamic interaction process accurately when the input parameters have been derived based on reference measurements. The ranges of intermittent crushing, frequency lock-in, and continuous brittle crushing, as shown in Fig. 14, match well given the natural variations occurring during experiments and not in the ideal numerical model. The predictions for the statistical measures of the

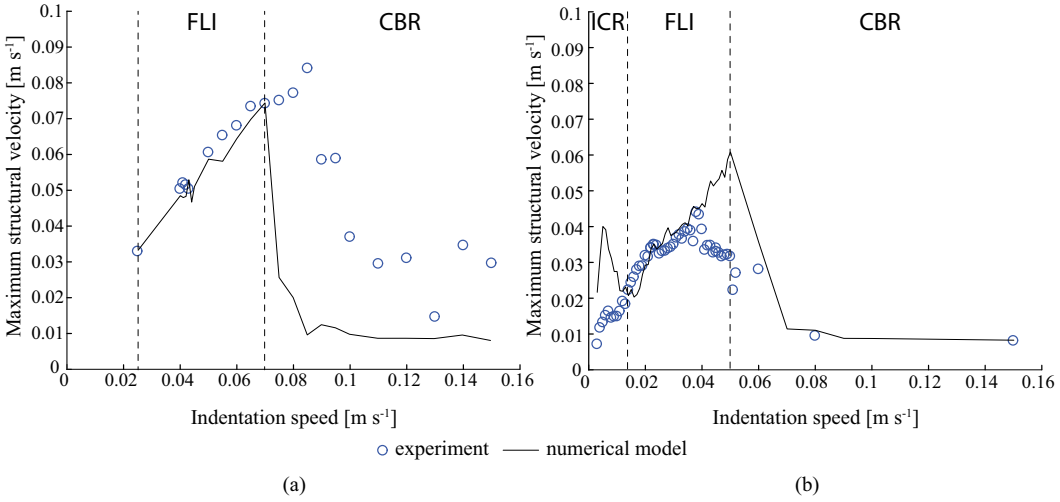

Fig. 14. Peak structure velocity in the direction of ice drift as a function of indentation speed as measured in the experiments and predicted by the model for compliant structure 1 (a), and 2 (b). The range of intermittent crushing (ICR), frequency lock-in (FLI), and continuous brittle crushing (CBR) from the model predictions are indicated by the dashed lines.

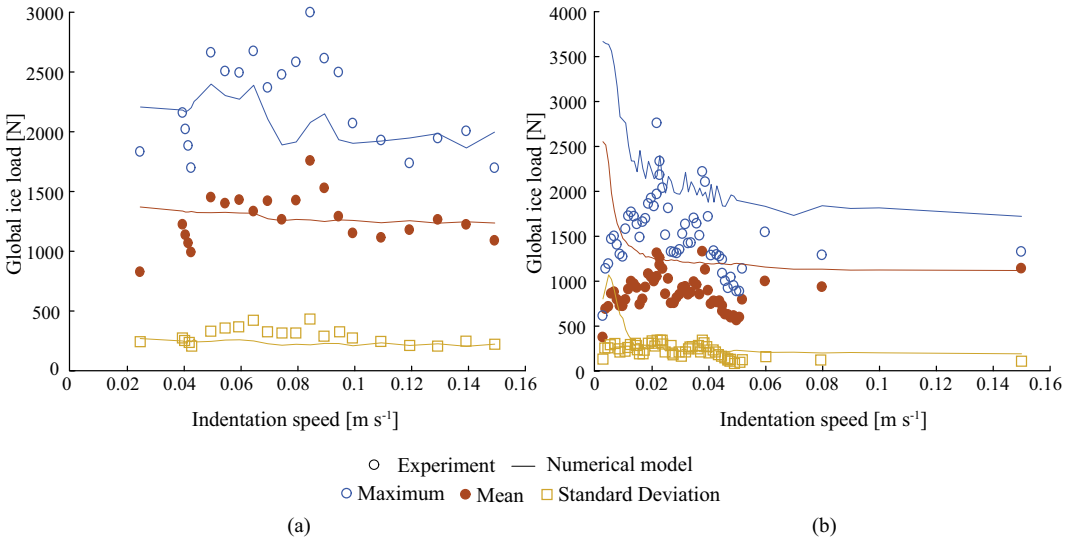

Fig. 15. Statistical measures of the global ice load as measured in the experiments and predicted by the model for compliant structure 1 (a), and compliant structure 2 (b).

structural displacements during frequency lock-in show strong correspondence to those observed in the experiments (see Fig. 16). In the continuous brittle crushing regime, the correspondence is weaker for which many reasons can be given, but one is clearly the influence of a higher mode of structural oscillation not included in the model but present in the experimental measurements (see Fig. 18). The detailed time histories in Fig. 17 show that the model captures the development of the global ice load in the lock-in range. The typical periodic pattern with an oscillation in between large load drops is seen in both experimental results and the model predictions.

The dependencies of the statistical measures of global load on indentation velocity, as shown in Fig. 15, match well for compliant structure 1. Both the model predictions and experimental measurements show an increase in statistical measures of the global load in the frequency lock-in range when compared to the brittle crushing range. For the test with compliant structure 1, a local hard-spot in the ice, indicated by the increase in mean global load in the range of 0.08 to 0.1 m s^{-1} in Fig. 15, illustrates the challenge in comparing model predictions and measurements if local variations in ice properties are not taken into account. For compliant structure 2 it is found that at low velocities the model predicts intermittent crushing to develop, resulting in an increase in global loads, whereas from experiments the load levels show to decrease. This can be explained by the influence of flexural ice motion and failure.

Sensitivity of the results with respect to the choice of input parameters is considered as some of the required reference measurements were not obtained, but estimated, from the rigid structure experiments. In Fig. 19, the model predictions for the maximum structural velocity in the direction of ice drift as a function of indentation speed are presented for five extreme cases of parameter estimations as defined in Table 6. For the cases where the maximum global load at the transition velocity is increased, case a, d and e, the limit for the indentation speed for which frequency lock-in is predicted to occur increases. For the cases where the opposite is true, case b and c, the limit for the indentation speed reduces. Note that with a change of the transition speed the estimate of the maximum global load changes based on the extrapolation applied (see Fig. 11). A larger amplitude for oscillation is predicted in the continuous brittle crushing range for the higher values of critical

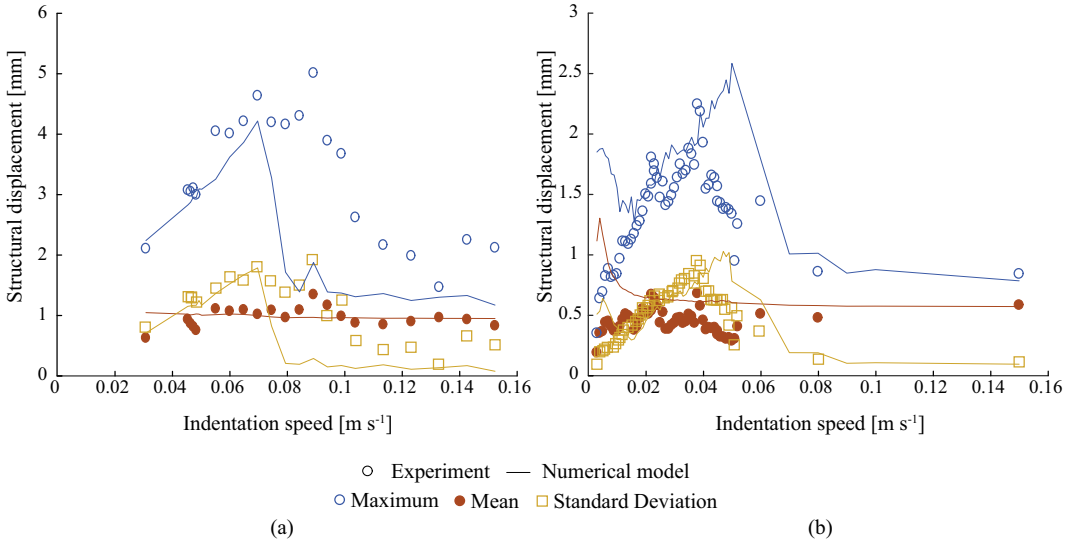

Fig. 16. Statistical measures of the structural displacement as measured in experiments and predicted by the model for compliant structure 1 (a), and compliant structure 2 (b).

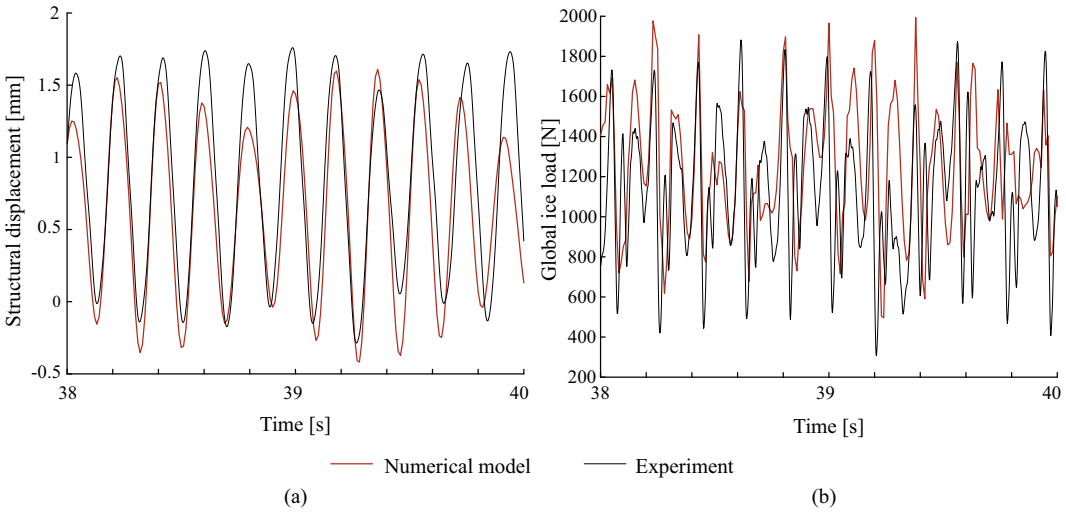

Fig. 17. Comparison of structural displacement (a) and global ice load (b) during frequency lock-in at an indentation speed of 0.023 m s^{-1} for compliant structure 2.

deformation, case b and d. In the frequency lock-in range the amplitude is unaffected by the choice of the critical deformation.

Regardless of the choice of parameters, frequency lock-in is predicted to develop over a range of indentation speeds for the extreme parameter choices. The maximum velocity for which lock-in is predicted to develop shows to vary by 0.03 m s^{-1} for the parameter ranges considered. In application of the model for design of offshore structures, the most conservative choice is to use a high estimate for the maximum global load and transition velocity. In application of the model for design of experiments, a lower estimate for the transition velocity and maximum global load can be used to maximize the chances of ice-induced vibrations developing at the intended indentation speeds.

7. Conclusion

Indentation experiments with rigid and compliant rectangular structures were conducted in model ice to gather data required for the validation of a model for prediction of dynamic ice-structure interaction. Based on the obtained data, an approach for determination of the model input parameters and the capability of the model to predict the interaction between ice and compliant structures are validated.

Dependencies of the statistical measures of the global ice load on indentation speed are obtained from the experiments with one rigid and two compliant structures. Information about the local failure behavior is obtained from tactile sensor measurements for all tests. The compliant structures experienced frequency lock-in over a range of velocities. The obtained measurement data can be used as a benchmark for validation of models for the prediction of dynamic ice-structure interaction.

The results from the experiments with the rigid structure are used to define the input parameters of the model. Due to the lack of data at low indentation speeds, some parameters had to be estimated. But a sensitivity study shows that, for the range of parameters considered, the effects on the model predictions are small. Future experiments focused on local contact and the transition between creep and crushing may allow for better estimates of these parameters. It is shown that the model captures the main trends observed in the global load dependence on indentation speed for rigid structures.

Using the input parameters defined based on the rigid structure experiments, the model has been applied to two scenarios of compliant structures interacting with ice. For both structures, experimental data have also been obtained. Comparison of the model predictions and experiments has shown that the model accurately captures the ranges of the different types of interaction and the structural oscillation pattern

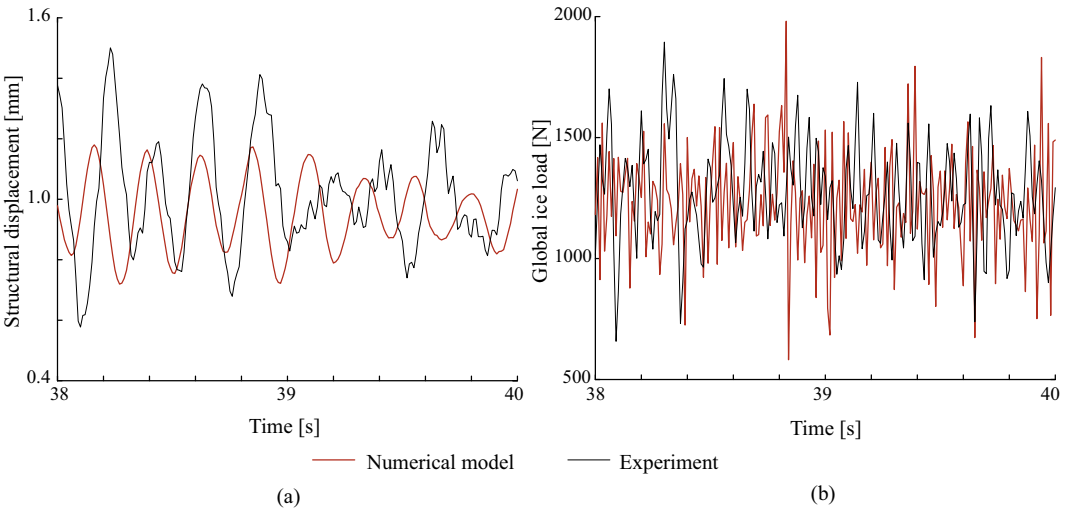

Fig. 18. Comparison of measured and predicted structural displacement (a) and global ice load (b) during continuous brittle crushing at a velocity of 0.13 m s^{-1} for compliant structure 1.

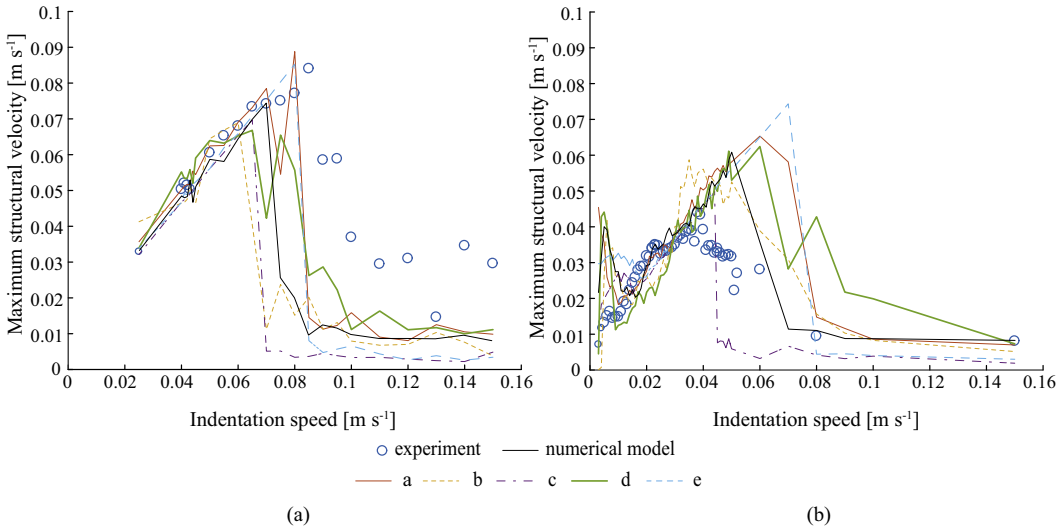

Fig. 19. Sensitivity of the predictions for the range of indentation speeds at which frequency lock-in develops for compliant structure 1 (a) and compliant structure 2 (b). Changes in the estimated parameters are defined in Table 6.

Table 6
Parameter estimates used for checking the sensitivity of the model predictions. Only the values which are changed with respect to the original estimates are presented.

Case	Parameter change
a	$\frac{F_{max,ref}}{F_{mean,ref}(v_{ice}\to\infty)} = 5$
b	$v_{t,ref} = 2$ mm s^{-1} $\delta_{f,ref} = 4$ mm
c	$v_{t,ref} = 2$ mm s^{-1} $\delta_{f,ref} = 0.5$ mm
d	$v_{t,ref} = 0.5$ mm s^{-1} $\delta_{f,ref} = 4$ mm
e	$v_{t,ref} = 0.5$ mm s^{-1} $\delta_{f,ref} = 0.5$ mm

within those ranges. Furthermore, the predicted global ice load dependence on time shows similar characteristics to that obtained from the experiments. The capability of the model to predict dynamic ice-structure interaction and the development of frequency lock-in and continuous brittle crushing has been validated. For intermittent crushing, additional experiments are required since the model ice used in the experiments experienced significant bending failure at low indentation speeds.

The presented approach for determining the input parameters of the model provides a guideline for application of the model to different model-scale and full-scale scenarios. Effects of changes in physical ice properties on the response of the ice have to be studied in more detail, but estimations can straightforwardly be implemented. Further studies aimed at the detailed development of local pressure and contact will allow for a refinement of the failure and contact in the phenomenological model.

Acknowledgements

The authors wish to acknowledge support from the Research Council of Norway (203471) through the Centre for Research-based Innovation SAMCoT and support from all SAMCoT partners. In particular, authors wish to thank partners involved in the IVOS project: DNV GL, Engie SA, Kvaerner AS, Multiconsult AS, Shell Technology Norway AS, and Total E&P Norge AS.

References

Bjork, B., 1981. Ice-Induced Vibration of Fixed Offshore Structures. Part 2: Experience With Baltic Lighthouses. Technical report. Ship Research Institute of Norway, Information Department.

Evers, K.-U., Jochmann, P., 1993. An advanced technique to improve the mechanical prop-erties of model ice developed at the HSVA ice tank. In: Proc. 12th International Conference on Port and Ocean Engineering Under Arctic Conditions, Hamburg. vol. 2. pp. 877–888.

Guo, F., 2013. Analysis of the key parameters in ice induced frequency lock-in. In: Proc. 22nd International conference on Port and Ocean Engineering under Arctic Conditions, POAC13-33.

Hendrikse, H., 2017. Ice-induced vibrations of vertically sided offshore structures. PhD thesis. Delft University of Technology.

Hendrikse, H., Metrikine, A., 2016. Ice-induced vibrations and ice buckling. Cold Reg. Sci. Technol. 131, 129–141.

Hinse, P., Müller, F., Ziemer, G., 2017. IVOS Progress Report April 2017. Technical Report. HSVA, Hamburg (41 p).

Huang, Y., Shi, Q., Song, A., 2007. Model test study of the interaction between ice and a compliant vertical narrow structure. Cold Reg. Sci. Technol. 49, 151–160.

ISO19906, 2010. Petroleum and Natural Gas Industries— Arctic Offshore Structures. International Organization for Standardization, Geneva.

Jefferies, M.G., Wright, W.H., 1988. Dynamic response of'Molikpaq' to ice-structure interaction. In: Proc. 7th International Conference on Offshore Mechanics and Arctic Engineering, Houston, Texas. vol. 4. pp. 201–220.

Ji, X., Oterkus, E., 2016. A dynamic ice-structure interaction model for ice-induced vibrations by using van der pol equation. Ocean Eng. 128, 147–152.

Kärnä, T., Kamesaki, K., Tsukuda, H., 1999. A numerical model for dynamic ice–structure interaction. Comput. Struct. 72, 645–658.

Määttänen, M.P., 1999. Numerical model for ice-induced vibration load lock-in and synchronization. In: Proc. 14th International Symposium on Ice, Potsdam. vol. 2. pp. 923–930.

Määttänen, M., Løset, S., Metrikine, A., Evers, K.-U., Hendrikse, H., Lønøy, C., Metrikin, I., Nord, T., Sukhorukov, S., 2012. Novel ice induced vibration testing in a large- scale facility: deciphering ice induced vibrations, part 1. In: Proc. 21st IAHR international Symposium on Ice, Dalian, China, pp. 946–958.

Palmer, A., Yue, Q., Guo, F., 2010. Ice-induced vibrations and scaling. Cold Reg. Sci. Technol. 60, 189–192.

Ponter, A.R.S., Palmer, A.C., Goodman, D.J., Ashby, M.F., Evans, A.G., Hutchinson, J.W., 1983. The force exerted by a moving ice sheet on an offshore structure part I. the creep mode. In: Cold Reg. Sci. Technol. 8. pp. 109–118.

Singh, S.K., Timco, G.W., Frederking, R.M.W., Jordaan, I.J., 1990. Tests of ice crushing on a flexible structure. In: Proc. 9th Offshore Mechanics and Arcitc Engineering Symposium, Houston, Texas. vol. 4. pp. 89–94.

Sodhi, D.S., 1994. An ice–structure interaction model. Mech. Geomater. Interfaces 57–75.

Sodhi, D.S., 2001. Crushing failure during ice-structure interaction. Eng. Fract. Mech. 68, 1889–1921.

Sodhi, D.S., Morris, C.E., 1984. Ice Forces on Rigid, Vertical, Cylindrical Structures. Report 84–33. US Army Cold Regions Research and Engineering Laboratory.

Takeuchi, T., Sakai, M., Akagawa, S., Nakazawa, N., Saeki, H., 2001. On the factors influencing the scaling of ice forces. In: Proc. IUTAM Symposium on Scaling Laws in Ice Mechanics and Ice Dynamics, Fairbanks, Alaska, pp. 149–160.

Timco, G.W., 1987. Indentation and penetration of edge-loaded freshwater ice sheets in the brittle range. J. Offshore Mech. Arct. Eng. 109 (3), 287–294.

Toyama, Y., Sensu, T., Minami, M., Yashima, N., 1983. Model tests on ice-induced self-excited vibration of cylindrical structures. In: Proc. 7th International Conference on Port and Ocean Engineering under Arctic Conditions, Helsinki, Finland. vol. 2. pp. 834–844.

Tsuchiya, M., Kanie, S., Ikejiri, K., Yoshida, A., Saeki, H., 1985. An experimental study on ice-structure interaction. In: Proc. 17th Annual Offshore Technology Conference, Houston, Texas, pp. 321–327.

Yue, Q.J., Li, L., 2003. Ice problems in Bohai Sea oil exploitation. In: Proc. 17th International Conference on Port and Ocean Engineering under Arctic Conditions, Trondheim, Norway, pp. 13.
Ziemer, G., 2016. IVOS Interim Report: Model Tests Phase 2.2: Series 24000, 25000 & 26000. Technical Report. Hamburgische Schiffbau-Versuchsanstalt (HSVA), Hamburg (18p).
Ziemer, G., 2017. Research Project IVOS – Ice-induced Vibrations of Offshore Structures. Technical Report. http://dx.doi.org/10.13140/RG.2.2.34529.40801. (4p).
Ziemer, G., Evers, K.-U., 2016. Model tests with a compliant cylindrical structure to investigate ice-induced vibrations. J. Offshore Mech. Arct. Eng. 138 (4) 8 p.